Check for updates

Journal of Microscopy, Vol. 209, Pt 1 January 2003, pp. 1–7
Received 1 August 2002; accepted 14 October 2002

SHORT COMMUNICATION

Evaluation of global analysis algorithms for single frequency fluorescence lifetime imaging microscopy data

P. J. VERVEER & P. I. H. BASTIAENS
Cell Biology and Cell Biophysics Programme, European Molecular Biology Laboratory, Meyerhofstrasse 1, D-69117 Heidelberg, Germany

Key words. Data fitting, FLIM, fluorescence microscopy, FRET, global analysis.

Summary

Global analysis of fluorescence lifetime image microscopy (FLIM) data can be used to obtain an accurate fit of multi-exponential fluorescence decays. In particular, it can be used to fit a bi-exponential decay to single frequency FLIM data, which is not possible with conventional fitting techniques. Bi-exponential fluorescence decay models can be used to analyse quantitatively single frequency FLIM data from samples that exhibit fluorescence resonance energy transfer (FRET). Global analysis algorithms simultaneously fit multiple measurements acquired under different experimental conditions to achieve higher accuracy. To demonstrate that bi-exponential models can indeed be fitted to single frequency data, we derive an analytical solution for the special case of two measurements and use this solution to illustrate the properties of global analysis algorithms. We also derive a novel global analysis algorithm that is optimized for single frequency FLIM data, and demonstrate that it is superior to earlier algorithms in terms of computational requirements.

Introduction

Fluorescence lifetime imaging microscopy (FLIM) can be used to spatially resolve the fluorescence lifetimes of one or more fluorescent probes (Lakowicz & Berndt, 1991; Gadella *et al.*, 1993; Bastiaens & Squire, 1999). Fluorescence lifetime provides information about the state and molecular environment of the probe. One process that can be monitored using FLIM is fluorescence resonance energy transfer (FRET). FRET is a non-radiative process where energy is transferred from an excited donor fluorophore to an acceptor fluorophore and then emitted as light if the distance between the fluorophores is sufficiently small (typically less than 10 nm; see Clegg, 1996). Because of this property, FRET has gained much popularity in the recent years as a tool for studying molecular binding in intact cells (Wouters *et al.*, 2001).

The direct transfer of energy from donor to acceptor represents an additional process by which the excited state of the donor can be depopulated, and therefore the fluorescence lifetime of the donor is reduced if FRET occurs (Bastiaens & Squire, 1999). Assuming a single exponential decay of the donor, the decay model in the presence of FRET is bi-exponential because, at each spatial position, the sample consists of two molecular species with distinct and different lifetimes, corresponding to 'bound' and 'unbound' states (Verveer *et al.*, 2001b). Quantitative analysis of FLIM data from samples that exhibit FRET thus requires the estimation of the lifetimes and the molar fractions of the two species.

Probably the simplest implementation of FLIM employs frequency domain techniques where the sample is illuminated with sinusoidally modulated light and the fluorescence light is measured with a detector that is modulated at the same frequency. Systematically shifting the phase of the detector modulation with respect to that of the illumination makes it possible to measure the phase shift and demodulation of the emitted fluorescent light (Clegg & Schneider, 1996; Bastiaens & Squire, 1999; Verveer *et al.*, 2001b). A single fluorescence lifetime can be estimated from either the measured modulation or the measured phase shift. These two estimations are independent and if the assumption of a single lifetime is correct they should be equal. If several molecular species with different lifetimes are present, these two estimations will differ. This provides some qualitative information about the composition of the sample, but the true lifetimes and relative amounts of each species cannot be determined without further information about the sample. For instance, if FRET occurs, at least two lifetimes must be estimated. In addition, the relative amount of molecules exhibiting FRET must be determined. Thus, in each pixel three parameters would need

Correspondence: P. I. H. Bastiaens. Tel.: +49 6221387 407; fax: +49 6221387 306; e-mail: bastiaen@embl-heidelberg.de

© 2003 The Royal Microscopical Society

to be estimated, whereas only two independent measurements are available. Hence, to apply single frequency FLIM measurements for the quantitative analysis of FRET data, additional information with appropriate data analysis techniques must be employed. In earlier work we therefore introduced the use of global analysis techniques to FLIM data (Verveer *et al.*, 2000a,b). Briefly, in global analysis data from several measurements from experiments under different conditions are analysed simultaneously. The knowledge that some parameters are invariant under the different experimental conditions is exploited to achieve a higher precision in the determination of these parameters (Beechem, 1992). In global analysis of FLIM data, the data in each pixel of the image are considered a different measurement, and therefore a single FLIM measurement consists of a large number of independent measurements. Under the right experimental conditions it can be assumed that the lifetimes are the same in each pixel (spatially invariant), and only the molar fractions (populations) of each species are different. A global analysis algorithm was derived for FLIM data, which determines the spatially invariant lifetimes with high accuracy, and also allows the calculation of the populations of each species. In our work we showed that this approach not only led to an increased accuracy in the estimation of lifetimes, but also that it is possible to fit models with twice the amount of lifetimes compared to a conventional pixel-by-pixel analysis. A direct consequence of this is that is becomes possible to fit a bi-exponential decay model to single frequency FLIM data. This approach was applied by us to FRET experiments, allowing a quantitative analysis that maps the relative concentration of molecules that do exhibit FRET compared to those that do not (Verveer *et al.*, 2000b, 2001a; Ng *et al.*, 2001). It should be noted that for every biological application it should be verified that the assumption of a spatial invariant bi-exponential decay is valid. An extensive treatment of this issue falls outside the scope of this short communication but can be found for our applications in an earlier publication (Verveer *et al.*, 2001a).

The previously presented global analysis algorithms were applicable to both single- and multiple-frequency FLIM data. Here, we further investigate global analysis algorithms for the special case of single frequency FLIM data. In our experience, it is not always well understood why the resolution of a bi-exponential decay model is possible with single frequency FLIM data. We therefore present an analytical solution for the case of two measurements, and use this to discuss the properties of global analysis of single frequency FLIM data. In addition we derive a specialized algorithm for single frequency FLIM data, and demonstrate that it is superior in terms of the use of computational resources to the previously published algorithm.

In single frequency FLIM the phase shift $\Delta\phi_i$ and modulation M_i of the fluorescent light are measured in each pixel i (Verveer *et al.*, 2001b). For convenience we transform these as follows:

$$A_i = M_i \sin(\Delta\phi_i), \tag{1a}$$

$$B_i = M_i \cos(\Delta\phi_i) \tag{1b}$$

In this work we assume that in addition to the phase shift $\Delta\phi_i$ and modulation M_i, estimations of the errors $\sigma_{\Delta\phi,i}$ and $\sigma_{M,i}$ are available. The errors in transformed values $\sigma_{A,i}$ and $\sigma_{B,i}$ can then be found by error propagation (Verveer *et al.*, 2001b).

Assuming that the FLIM instrument operates at a single circular frequency ω, it can be shown (Verveer *et al.*, 2001b) that A_i and B_i are related to the lifetimes and the fractional fluorescence of each species by:

$$A_i = \sum_{q=1}^{Q} \frac{\omega\tau_q\alpha_{q,i}}{1+\omega^2\tau_q^2}, \tag{2a}$$

$$B_i = \sum_{q=1}^{Q} \frac{\alpha_{q,i}}{1+\omega^2\tau_q^2}, \tag{2b}$$

where Q different species of molecules with distinct lifetimes τ_q are assumed to be present in the sample, and $\alpha_{q,i}$ is the relative contribution of the qth species to the total fluorescence intensity in the ith pixel. The $\alpha_{q,i}$ obey the constraint:

$$\sum_{q=1}^{Q} \alpha_{q,i} = 1. \tag{3}$$

To obtain the population of each species, $\alpha_{q,i}$ must be renormalized by their relative quantum yields. Note that these equations are linear in α_i, and, therefore, if τ_i are known, the α_i can be determined by a linear estimation method, as discussed by Verveer *et al.* (2000a, 2001b). Therefore, for the present discussion, it is sufficient to concentrate on the estimation of the lifetimes. In fact, the linearity can be exploited to reduce the parameter estimation problem as we will demonstrate now, first with an analytical solution for two measurements and then for a numerical algorithm for an arbitrary number of measurements.

Estimation of the lifetimes

Analytical solution for two measurements

We assume a bi-exponential system, and rewrite Eq. (2) as follows:

$$A_i = \frac{\omega\tau_1\alpha_{1,i}}{1+\omega^2\tau_1^2} + \frac{\omega\tau_2(1-\alpha_{1,i})}{1+\omega^2\tau_2^2}, \tag{4a}$$

$$B_i = \frac{\alpha_{1,i}}{1+\omega^2\tau_1^2} + \frac{1-\alpha_{1,i}}{1+\omega^2\tau_2^2}, \tag{4b}$$

where we used the constraint given by Eq. (3) to eliminate $\alpha_{2,i}$. We assume two distinct measurements where the lifetimes τ_1 and τ_2 remain unchanged, but where the fluorescence fractions are different: $\alpha_{1,1} \neq \alpha_{1,2}$. Thus, we have two measurements A_1, B_1 and A_2, B_2, and we can derive two equalities that are independent of the fractional contributions $\alpha_{1,1}$ and $\alpha_{1,2}$:

13652818, 2003, 1, Downloaded from https://onlinelibrary.wiley.com/doi/10.1046/j.1365-2818.2003.01093.x by University College London UCL Library Services, Wiley Online Library on [26/01/2024]. See the Terms and Conditions (https://onlinelibrary.wiley.com/terms-and-conditions) on Wiley Online Library for rules of use; OA articles are governed by the applicable Creative Commons License

$$\frac{A_1 - A_2}{B_1 - B_2} = \frac{\omega^2\tau_1\tau_2 - 1}{\omega(\tau_1 + \tau_2)} \text{ and } \frac{A_1 - \dfrac{\omega\tau_2}{1+\omega^2\tau_2^2}}{B_1 - \dfrac{1}{1+\omega^2\tau_2^2}} = \frac{\omega^2\tau_1\tau_2 - 1}{\omega(\tau_1 + \tau_2)}. \quad (5)$$

Hence, it follows that

$$\frac{(1+\omega^2\tau_2^2)A_1 - \omega\tau_2}{(1+\omega^2\tau_2^2)B_1 - 1} = \frac{A_1 - A_2}{B_1 - B_2}, \quad (6)$$

from which we find, after some rearrangements, a quadratic equation where one of the lifetimes has been eliminated:

$$(A_2B_1 - A_1B_2)\omega^2\tau_2^2 - (B_1 - B_2)\omega\tau_2 + A_2B_1 - A_1B_2 + A_1 - A_2 = 0, \quad (7)$$

which has two solutions:

$$\tau_2 = \frac{1}{\omega} \cdot \frac{B_1 - B_2 \pm \sqrt{(B_1 - B_2)^2 - 4(A_2B_1 - A_1B_2)(A_2B_1 - A_1B_2 + A_1 - A_2)}}{2(A_2B_1 - A_1B_2)}. \quad (8)$$

Given one of these two solutions for τ_2, it is straightforward to show that τ_1 is given by the other solution, by substitution into Eq. (5). Thus, given two measurements we can calculate the two lifetimes. Unfortunately, we were not able to prove analytically that these two solutions are real. That is, we could not prove that the determinant $(B_1 - B_2)^2 - 4(A_2B_1 - A_1B_2)(A_2B_1 - A_1B_2 + A_1 - A_2)$ is always greater than or equal to zero. For this reason we resorted to numerical simulations to show that this is the case for realistic values of τ_1, τ_2, $\alpha_{1,1}$ and $\alpha_{1,2}$. These simulations are discussed in more detail in the results section below.

Equation (8) does not have much practical value for large sets of FLIM data, but it does demonstrate that, assuming invariant lifetimes, single frequency FLIM data can be analysed in terms of a bi-exponential model, provided that we analyse multiple measurements simultaneously. This analytical equation can also be used to qualitatively understand the behaviour of these algorithms. For instance, consider what happens if $\alpha_{1,1} = \alpha_{1,2}$. In this case $A_1 = A_2$ and $B_1 = B_2$, the denominator of Eq. (8) is zero, and the solution does not exist. Even if $\alpha_{1,1}$ and $\alpha_{1,2}$ are not equal, but close to each other, then $A_1 \approx A_2$ and $B_1 \approx B_2$, leading to a solution that is unstable, or, if the determinant becomes smaller than zero, non-existent. This provides an explanation of why global analysis of single frequency is only useful if sufficient variation is present in the sample, i.e. there must be sufficient spatial variation in the molar fractions of the bound and unbound species. A similar reasoning can be applied to the case where the two lifetimes, rather than the $\alpha_{1,i}$, are equal or close to each other. In such a case, $A_1 \approx A_2$ and $B_1 \approx B_2$ and the solution becomes unstable. In general, how well the fractions and/or the lifetimes must be separated to be able to successfully apply the single frequency global analysis depends on factors such as signal-to-noise ratio and measurement frequency.

Global analysis of an arbitrary number of measurements

For a practical implementation of single frequency global analysis of N points, a least-squares approach is taken. The algorithm described by Verveer *et al.* (2000a) utilized a truncated Newton algorithm (Schlick & Fogelson, 1992) to minimize a χ^2 function over all τ_i and $\alpha_{1,i}$, a total of $Q + N(Q-1)$ parameters, leading to a computationally expensive algorithm because the N can easily be as large as several million measurements. More recently we have been exploiting the partial linear nature of the χ^2 function to reduce the dimensionality of the minimization problem. In this scheme the minimization is done by a Levenberg–Marquardt algorithm (Press *et al.*, 1992) over the Q lifetimes only. At each evaluation of the χ^2 function, the $\alpha_{q,i}$ are estimated using singular value decomposition (SVD; Press *et al.*, 1992) using the current estimate of the lifetimes. Thus, the dimensionality of the minimization problem is reduced to be equal to the number of lifetimes Q, rather than $Q + N(Q-1)$. As the χ^2 is partially evaluated numerically, analytical expressions for the derivatives are not available, but the use of numerical derivatives proved to be very effective in this case. Due to the reduced amount of parameters, this approach is far more efficient than the brute-force approach using a truncated Newton algorithm, while providing the same results. This algorithm has been used routinely in our laboratory for the last two years and has proven to be very reliable. However, for the special case of single frequency FLIM data it is possible to derive an even more optimized approach. To this end we define the following χ^2 function:

$$\chi^2(\tau_1,\tau_2,\alpha_{1,i}) = \sum_{i=1}^{N}\left[\frac{1}{\sigma_{A,i}^2}\left(A_i - \frac{\omega\tau_1\alpha_{1,i}}{1+\omega^2\tau_1^2} - \frac{\omega\tau_2(1-\alpha_{1,i})}{1+\omega^2\tau_2^2}\right)^2 + \frac{1}{\sigma_{B,i}^2}\left(B_i - \frac{\alpha_{1,i}}{1+\omega^2\tau_1^2} - \frac{(1-\alpha_{1,i})}{1+\omega^2\tau_2^2}\right)^2\right]. \quad (9)$$

Because this function is quadratic in $\alpha_{1,i}$ we can find an explicit expression for the $\alpha_{1,i}$ in terms of the lifetimes by linear minimization with respect to $\alpha_{1,i}$:

$$\alpha_{1,i} = \frac{(1+\omega^2\tau_1^2)(\omega(\tau_1+\tau_2)((1+\omega^2\tau_2^2)B_i - 1)\sigma_{A,i}^2 + (\omega^2\tau_1\tau_2 - 1)((1+\omega^2\tau_2^2)A_i - \omega\tau_2)\sigma_{B,i}^2)}{\omega(\tau_2 - \tau_1)(\omega^2(\tau_1+\tau_2)^2\sigma_{A,i}^2 + (\omega^2\tau_1\tau_2 - 1)^2\sigma_{B,i}^2)}. \quad (10)$$

13652818, 2003, 1, Downloaded from https://onlinelibrary.wiley.com/doi/10.1046/j.1365-2818.2003.01093.x by University College London UCL Library Services, Wiley Online Library on [26/01/2024]. See the Terms and Conditions (https://onlinelibrary.wiley.com/terms-and-conditions) on Wiley Online Library for rules of use; OA articles are governed by the applicable Creative Commons License

Substituting this expression back into Eq. (9) we get a reduced function that can be simplified to the following expression:

$$\chi^2(\tau_1,\tau_2) = \sum_{i=1}^{N} \frac{((\omega^2\tau_1\tau_2 - 1)B_i - \omega(\tau_1 + \tau_2)A_i + 1)^2}{\omega^2(\tau_1 + \tau_2)^2\sigma_{A,i}^2 + (\omega^2\tau_1\tau_2 - 1)^2\sigma_{B,i}^2}. \quad (11)$$

Minimizing this function over τ_1 and τ_2 yields the estimated lifetimes. These can then be substituted in Eq. (10) to find the $\alpha_{1,i}$. In principle, the derivatives of this reduced functional can be found analytically and employed in any gradient-based minimization algorithm. In practice we use a Levenberg–Marquardt algorithm with numerical derivatives.

Results

Numerical analysis of the analytical solution

The analytical solution given by Eq. (8) gives two solutions. However, we were not able to prove that these solutions are real, by showing that the determinant is larger than or equal to zero:

$$(B_1 - B_2)^2 - 4(A_2B_1 - A_1B_2)(A_2B_1 - A_1B_2 + A_1 - A_2) \geq 0. \quad (12)$$

Obviously, in the presence of noise, when $A_1 \approx A_2$ and $B_1 \approx B_2$, this inequality may be violated. However, the question arises whether in the absence of noise this inequality still holds. To investigate this numerically for realistic values of the two lifetimes we performed simulations by randomly selecting values for τ_1 and τ_2 from a uniform distribution between 0.1 and 4.0 ns, and values of $\alpha_{1,1}$ and $\alpha_{1,2}$ from a uniform distribution between 0.0 and 1.0. The random values were rejected if $\tau_1 - \tau_2 < 10^{-4}$ or $\alpha_{1,1} - \alpha_{1,2} < 10^{-4}$, as such close values lead to instabilities in the solution due to roundoff errors. Using these random values, the corresponding values for A_1, A_2, B_1 and B_2 were calculated and the inequality (12) was tested. This test was repeated 10^8 times. We found only 11 violations of the inequality, where in all cases both $\tau_1 - \tau_2$ and $\alpha_{1,1} - \alpha_{1,2}$ were close to zero, and the absolute value of the determinant was less than 10^{-23}. We therefore ascribed these violations to numerical roundoff errors, and are confident that for this range of values of the lifetimes, the solutions of the analytical Eq. (8) exist.

Comparison of different implementations of global analysis

We compared three different implementations of global analysis for single frequency FLIM measurements: (1) the implementation described by Verveer *et al.* (2000a) that employs a brute-force approach using a truncated Newton minimization, denoted by 'global-TN'; (2) the implementation that employs Levenberg–Marquardt minimization using singular value decomposition to substitute the $\alpha_{1,i}$ numerically, described in the previous section and denoted by 'global-SVD'; (3) the new algorithm for single frequency FLIM data introduced in this paper, that minimizes the analytically derived reduced function, denoted by 'global-SF'. Given the lifetimes, the fluorescence fractions $\alpha_{1,i}$ can be obtained separately by linear estimation, but each algorithm uses a different approach to take the fluorescence fractions into account. The global-TN algorithm estimates the fluorescence fractions simultaneously with the lifetimes. The other two algorithms do not directly calculate the fluorescence fractions, and these must be calculated separately. As the global-SVD algorithm uses a singular value decomposition to eliminate the $\alpha_{1,i}$, we used linear estimation by SVD decomposition to calculate the fluorescence fractions after substitution of the estimated lifetimes into Eqs (2) and (3) and (see also Verveer *et al.*, 2000a). In the case of the global-SF algorithm the fluorescence fractions are eliminated analytically using Eq. (10) and we therefore used this expression to calculate the fluorescence fractions.

To establish that these algorithms essentially calculate the same results we performed simulations over a range of lifetime values, and for different levels of noise. The simulated test object is similar to that described by Verveer *et al.* (2000a): an image of $M \times M$ pixels was generated with $\alpha_{1,i} = i/(M \times M)$, where i was the number of the pixel, counting in a one-dimensional fashion from the upper left to the lower right corner of the image. Using this image for the fractional contributions to the fluorescence, phase-dependent single-frequency data with a frequency of 80 MHz was generated, and Poisson noise was added to the simulated data. To control the signal-to-noise ratio, the average intensity of the data sequence was varied. From these simulated data, the demodulations and phase-shifts with error estimations were calculated in each pixel using a linear estimation (Verveer *et al.*, 2000a). In our implementations of global-TN and global-SVD these are directly used as inputs. In the case of global-SF, we first calculated A_1 and B_1 from the estimated demodulations and phase shifts using Eq. (1) and their errors by error propagation (Verveer *et al.*, 2001b) and then determined the lifetimes by minimizing Eq. (11) using a Levenberg–Marquardt algorithm. We refer to Verveer *et al.* (2000a) for detailed information about the generation of this simulated data. The algorithms were executed on a PC equipped with a 733 MHz Pentium III processor and 1 Gb of memory, running the Linux operating system. The simulations were repeated 25 times with different realizations of the noise, and the mean and standard deviations of the results were plotted.

Figure 1 shows the fitted lifetimes for simulations of 10×10 images where the first lifetime (τ_1) was fixed to 2.0 ns, and the second lifetime component (τ_2) was varied from 1.1 to 1.7 ns. Figures 1(A)–(C) show the results for global-TN, global-SVD and global-SF, respectively. All three algorithms yield similar results and are capable of fitting the lifetimes well as long as the difference between the two lifetimes is sufficiently large. The difference between lifetimes that still can be resolved

13652818, 2003, 1, Downloaded from https://onlinelibrary.wiley.com/doi/10.1046/j.1365-2818.2003.01093.x by University College London UCL Library Services, Wiley Online Library on [26/01/2024]. See the Terms and Conditions (https://onlinelibrary.wiley.com/terms-and-conditions) on Wiley Online Library for rules of use; OA articles are governed by the applicable Creative Commons License

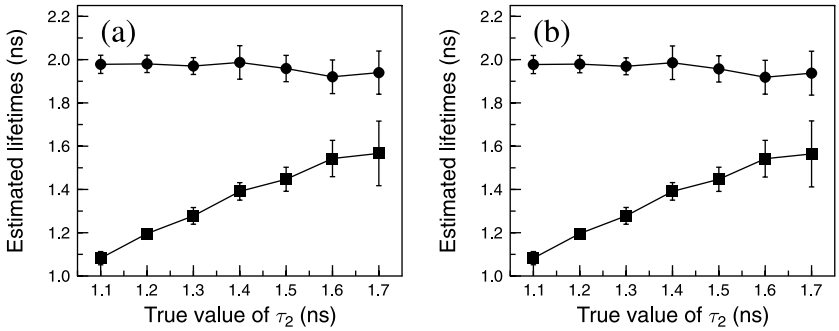

Fig. 1. Estimated values of τ_1 and τ_2 as a function of the true value of τ_2 for the different fitting approaches on single frequency FLIM data. Shown are average estimated values and standard deviations for τ_1 (●) and τ_2 (■) calculated from 25 data sets with different realizations of Poisson noise. If a point shows no error bars, the standard deviation was too small to be plotted. (a) 10×10 $\alpha_{1,i}$ image, average intensity = 300 counts, global-TN; (b) 10×10 $\alpha_{1,i}$ image, average intensity = 300 counts, global-SVD; (c) 10×10 $\alpha_{1,i}$ image, average intensity = 300 counts, global-SF. (d) 64×64 $\alpha_{1,i}$ image, average intensity = 3000 counts, global-SF algorithm.

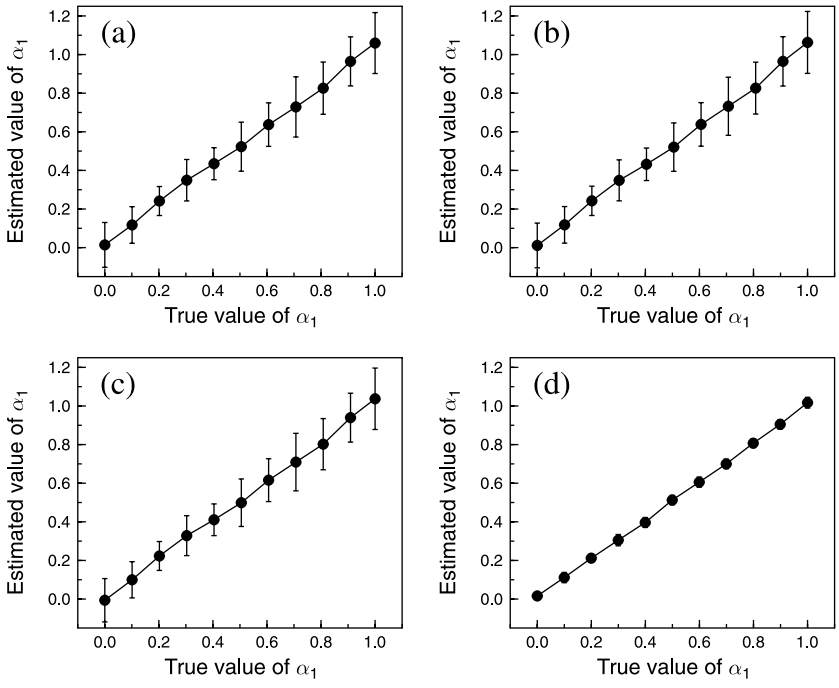

Fig. 2. Estimated values of the fluorescence fractions α_1, as a function of the true fluorescence fractions for the different fitting approaches on single frequency FLIM data, for true lifetime values of $\tau_1 = 2.0$ and $\tau_2 = 1.4$ ns. The simulated data are the same as that from Fig. 1 ($\tau_2 = 1.4$ ns data points). Shown are average estimated values and standard deviations calculated from 25 data sets with different realizations of Poisson noise. If a point shows no error bars, the standard deviation was too small to be plotted. For clarity, only 10 points from each 10×10 or 64×64 $\alpha_{1,i}$ image are plotted. (a) 10×10 $\alpha_{1,i}$ image, average intensity = 300 counts, global-TN; (b) 10×10 $\alpha_{1,i}$ image, average intensity = 300 counts, global-SVD; (c) 10×10 $\alpha_{1,i}$ image, average intensity = 300 counts, global-SF. (d) 64×64 $\alpha_{1,i}$ image, average intensity = 3000 counts, global-SF algorithm.

experimentally is dependent on the signal-to-noise ratio in the data, and the number of data points that are used in the global analysis. Here we deliberately chose a small test image, and used a low average intensity of the phase-dependent data (300 counts) in order to generate visible error bars for the purpose of comparing the behaviour of the three algorithms. As a consequence, the estimated lifetime values were not correct for small differences of the true lifetime values. Generally, much bigger data sets with better noise statistics are fitted and the results are more precise. This is illustrated in Fig. 1(D), which gives the result of global-SF for a bigger image (64×64 pixels) with simulated data that have a higher average intensity (3000 counts). The resulting fits are much more precise: the standard deviations are so small that the error-bars are not visible. In addition, the results are also correct for smaller differences between the two lifetimes. Figure 2 shows the

13652818, 2003, 1, Downloaded from https://onlinelibrary.wiley.com/doi/10.1046/j.1365-2818.2003.01093.x by University College London UCL Library Services, Wiley Online Library on [26/01/2024]. See the Terms and Conditions (https://onlinelibrary.wiley.com/terms-and-conditions) on Wiley Online Library for rules of use; OA articles are governed by the applicable Creative Commons License

Table 1. Summary of the performance of the three global analysis algorithms applied to a set of 30 FLIM sequences of MCF7 cells transfected with ErbB1-GFP, stimulated with EGF, and after fixation, incubated with a Cy3-labelled antibody against phosphotyrosine.

Algorithm	Memory usage (Mb)	Execution time (s)	τ_1 (ns)	τ_2 (ns)
Global-TN	100	1295	2.28	0.72
Global-SVD	92	40	2.28	0.72
Global-SF	61	13	2.29	0.74

fluorescence fractions α_1 for the case of $\tau_2 = 1.4$ ns. Again, it is clear that the three algorithms perform similarly.

To illustrate the use of a large real data set, we applied each algorithm to a biological application that has been studied extensively in our laboratory (Wouters & Bastiaens, 1999; Verveer *et al.*, 2000b). The samples consist of MCF7 cells grown on coverslips, transfected with the epidermal growth factor receptor ErbB1-GFP, stimulated for 2 min with epidermal growth factor (EGF), fixed with paraformaldehyde, permeabilized with 0.1% TX100, and then incubated with a Cy3-labelled antibody against phosphotyrosine (Cy3-PY72). Upon stimulation with EGF, the ErbB1 receptors are phosphorylated, a state that can be detected by FRET between the GFP fused to the receptor and the Cy3-labelled antibody that binds to the phosphorylation sites. Because the ErbB1-GFP has, in approximation, a single exponential decay, and the geometry of binding of the antibodies is fixed, it is expected that the sample consists of a mixture of two species with distinct lifetimes, and that fitting a bi-exponential decay model is appropriate (Verveer *et al.*, 2001a). See Verveer *et al.* (2000b) for a description of this application and Verveer *et al.* (2001b) for a detailed description of the data analysis. The data consisted of 30 FLIM image sequences, containing a total of 69 different cells. The sequences were pre-processed as described by Verveer *et al.* (2001b). Only pixels of interest within the boundaries of the cells were selected for analysis, yielding a total of approximately one million pixels in which the populations had to be estimated. The application of the three algorithms to these data yielded similar results (see Table 1) that corresponded to the lifetime values obtained in our earlier work. There is a small difference of 10–20 ps in the estimated value, which we ascribe to the fact that the global-SF algorithm minimizes a function that is rather different in shape to the function minimized by the two other algorithms. Hence, depending on tolerance settings of the algorithm, slightly different values were found. The resulting population images were essentially identical and we refer to our earlier publications for examples of such an image (Verveer *et al.*, 2000b, 2001a,b). Because the algorithms provide essentially the same results, it is of interest to compare the relative computational requirements of the algorithms. Table 1 shows the maximum use of physical memory, as measured by a Linux system tool, the time needed to execute the program, and the estimated lifetimes. It is clear that the new algorithm described in this paper performs best in terms of computational requirements.

Conclusions

In this paper we discussed the use of global analysis algorithms applied to single frequency FLIM data. We derived an analytical solution for the case of two measurements, and used it to illustrate the behaviour of this type of algorithm. This demonstrates that global analysis of single frequency FLIM data allows fitting of a bi-exponential model, as long as sufficient variation in the molar fractions of each species is present. Such variation is usually easily achieved experimentally by using FLIM data from control samples. Furthermore, we derived a practical algorithm that is optimized for single frequency FLIM data, and showed that this new algorithm is superior in terms of its computational requirements, compared to the algorithms that were in use before. Finally, we note that the new algorithm presented here is considerably easier to implement than the previous algorithms.

Acknowledgements

P.J.V. is the recipient of a Marie Curie fellowship from the European Union. We thank Dr Anthony Squire for critically reading the manuscript.

References

Bastiaens, P.I.H. & Squire, A. (1999) Fluorescence lifetime imaging microscopy: spatial resolution of biochemical processes in the cell. *Trends Cell Biol.* **9**, 48–52.

Beechem., J.M. (1992) Global analysis of biochemical and biophysical data. *Meth. Enzymol.* **210**, 37–54.

Clegg, R.M. (1996) Fluorescence resonance energy transfer. *Fluorescence Imaging Spectroscopy and Microscopy* (ed. by X.F. Wang & B. Herman), pp. 179–252. Wiley, New York.

Clegg, R.M. & Schneider, P.C. (1996) Fluorescence lifetime-resolved imaging microscopy: a general description of lifetime-resolved imaging measurements. *Fluorescence Microscopy and Fluorescence Probes* (ed. by J. Slavik), pp. 15–33. Plenum Press, New York.

Gadella, T.W.J., Jr, Jovin, T.M. & Clegg, R.M. (1993) Fluorescence lifetime imaging microscopy (FLIM) – spatial-resolution of microstructures on the nanosecond time-scale. *Biophys. Chem.* **48**, 221–239.

Lakowicz, J.R. & Berndt, K. (1991) Lifetime-selective fluorescence imaging using an rf phase-sensitive camera. *Rev. Sci. Instrum.* **62**, 1727–1734.

Ng, T., Parsons, M., Hughes, W.E., Monypenny, J., Zicha, D., Gautreau, A., Arpin, M., Gschmeissner, S., Verveer, P.J., Bastiaens, P.I.H. & Parker, P.J. (2001) Ezrin is a downstream effector of trafficking PKC-integrin complexes involved in the control of cell motility. *EMBO J.* **20**, 2723–2741.

Press, W.H., Teukolsky, S.A. & Vetterling, W.T. (1992) *Numerical Recipes in C*, 2nd edn. Cambridge University Press, Cambridge.

Schlick, T. & Fogelson, A. (1992) TNPACK – a truncated Newton minimization package for large-scale problems: I. Algorithm and usage. *ACM Trans. Math. Soft.* **18**, 46–70.

13652818, 2003, 1, Downloaded from https://onlinelibrary.wiley.com/doi/10.1046/j.1365-2818.2003.01093.x by University College London UCL Library Services, Wiley Online Library on [26/01/2024]. See the Terms and Conditions (https://onlinelibrary.wiley.com/terms-and-conditions) on Wiley Online Library for rules of use; OA articles are governed by the applicable Creative Commons License

Verveer, P.J., Squire, A. & Bastiaens, P.I.H. (2000a) Global analysis of fluorescence lifetime imaging microscopy data. *Biophys. J.* **78**, 2127–2137.

Verveer, P.J., Squire, A. & Bastiaens, P.I.H. (2001a) Improved spatial discrimination of protein reaction states in cells by global analysis and deconvolution of fluorescence lifetime imaging microscopy data. *J. Microsc.* **202**, 451–456.

Verveer, P.J., Squire, A. & Bastiaens, P.I.H. (2001b) Frequency domain fluorescence lifetime imaging microscopy. A window on the biochemical landscape of the cell. *Methods in Cellular Imaging* (ed. by A. Periasamy), pp. 273–294. Oxford University Press, Oxford.

Verveer, P.J., Wouters, F.S., Reynolds, A.R. & Bastiaens, P.I.H. (2000b) Quantitative imaging of lateral ErbB1 receptor signal propagation in the plasma membrane. *Science*, **290**, 1567–1570.

Wouters, F.S. & Bastiaens, P.I.H. (1999) Fluorescence lifetime imaging of receptor tyrosine kinase activity in cells. *Current Biol.* **9**, 1127–1130.

Wouters, F.S., Verveer, P.J. & Bastiaens, P.I.H. (2001) Imaging biochemistry inside cells. *Trends Cell Biol.* **11**, 203–211.

13652818, 2003, 1, Downloaded from https://onlinelibrary.wiley.com/doi/10.1046/j.1365-2818.2003.01093.x by University College London UCL Library Services, Wiley Online Library on [26/01/2024]. See the Terms and Conditions (https://onlinelibrary.wiley.com/terms-and-conditions) on Wiley Online Library for rules of use; OA articles are governed by the applicable Creative Commons License